Ab initio potential energy surfaces and spectroscopic and radiative properties of the low-lying states of the radium monohydroxide RaOH radical

Yuliya Osika , Sergey Sharashkin , George Pitsevich , Maksim Shundalau

PII: S0022-4073(23)00370-9
DOI: https://doi.org/10.1016/j.jqsrt.2023.108852
Reference: JQSRT 108852

To appear in: *Journal of Quantitative Spectroscopy & Radiative Transfer*

Received date: 7 July 2023
Revised date: 28 November 2023
Accepted date: 29 November 2023

Please cite this article as: Yuliya Osika , Sergey Sharashkin , George Pitsevich , Maksim Shundalau , Ab initio potential energy surfaces and spectroscopic and radiative properties of the low-lying states of the radium monohydroxide RaOH radical, *Journal of Quantitative Spectroscopy & Radiative Transfer* (2023), doi: https://doi.org/10.1016/j.jqsrt.2023.108852

Highlights

- Fock-space relativistic coupled cluster calculations
- Potential energy surfaces
- Molecular spectroscopic constants
- Radiative properties
- Laser cooling schem

Ab initio potential energy surfaces and spectroscopic and radiative properties of the low-lying states of the radium monohydroxide RaOH radical

Yuliya Osika [a], Sergey Sharashkin [a], George Pitsevich [a], Maksim Shundalau [b]*

[a] *Faculty of Physics, Belarusian State University, Minsk, Belarus*
[b] *Department of Information and Electrical Engineering and Applied Mathematics, University of Salerno, Fisciano, Italy*

** Corresponding author, e-mail: mshundalau@unisa.it*

Abstract. Herein, we present the state-of-the-art *ab initio* studies of the lower states of radium monohydroxide RaOH radical and its deuterated RaOD isotopologue. The potential energy surfaces of the ground and five low-lying excited states are calculated using the Fock-space relativistic coupled cluster method. The vibrational energy levels and all the fundamental frequencies are calculated for the first time using the potential energy surfaces and taking into account the interaction of the modes. Spectroscopic parameters such as electronic term energies, equilibrium internuclear distances, transition and permanent dipole moments, Franck–Condon factors, and radiative lifetimes are predicted. The probable vibrational laser cooling schemes are also proposed.

Keywords. Fock-space coupled cluster calculations; radium monohydroxide RaOH molecule; Potential energy surfaces; Radiative lifetimes; Vibrational states; Franck–Condon factors; Direct laser cooling

1. Introduction

During the last decades, the unique properties of ultracold molecules are considered to be used for detection of space parity violating (*P*-odd effects) as well as both space parity and time-reversal violating (*P*-, *T*-odd effects) [1, 2]. The ultralow temperatures of rarefied molecular gases can be reached using laser cooling methods, including direct laser cooling [1]. Note that measured parameters critically depend on the atomic mass, and thus, for these goals it is preferable to use heavy atoms, which often do not have stable isotopes. Conditions for the realization of direct laser cooling [3] require an optical cycling center (OCC), which usually includes an alkaline earth metal atom and a halide atom (e.g., F) or a pseudohalide functional group (e.g., –OH or $–OCH_3$). Recently, the simplest (i.e., diatomic) molecules with OCC, strontium monofluoride SrF [4, 5] and calcium monofluoride CaF [6, 7] radicals, were successfully cooled using mentioned method. Regarding the search of *P*-odd and *P*-, *T*-odd effects, polyatomic molecules, and linear triatomic ones, in particular, have some advantages before diatomics due to the *l*-doubling effect [8], which is expected to improve the sensitivity of future experiments on searching for space parity and time-reversal violating (for details see recent review [9]). Very recently linear triatomic CaOH [10, 11], SrOH [12], and YbOH [13] radicals were successfully laser cooled.

Radium-containing compounds with OCC have at least two advantages before other alkaline earth metal analogues: the largest mass of the radium atom and the highest degree of diagonality of vibronic transitions [14, 15]. Isaev et al. [16] for the first time considered RaOH as a promising molecule for direct laser cooling. In contrast to numerous experimental studies of other linear alkaline earth metal monohydroxides (CaOH/CaOD [17–26], SrOH [20, 27–33], BaOH/BaOD [20, 34–40], and similar YbOH [25, 41–46] molecule), to the best of our knowledge, only one experimental study has been directly related to radium monohydroxide. Namely, Fan et al. [47] applied an all-optical mass spectrometry technique to identify the first controlled synthesis of $RaOH^+$ ions.

Isaev et al. [16] predicted the energy of the first excited $\tilde{A}^2\Pi_{1/2}$ state of the RaOH, geometric parameters of the molecule in the ground $\tilde{X}^2\Sigma^+$ and first excited states, harmonic frequencies, permanent and transition dipole moments (PDMs and TDMs) and estimated the parameters of the *P*-odd and *P*-, *T*-odd effects based on the calculations at the MCSCF and FS-RCCSD levels of theory. Isaev et al. [16] also evaluated the Franck–Condon factors (FCFs) for the $\tilde{A}^2\Pi_{1/2} \rightarrow \tilde{X}^2\Sigma^+$ channel. Note that the latter calculations are based on the model of the RaX diatomic quasimolecule, where X is considered as an OH quasiatom [16]. Based on the CCSD level of theory, Vasiliu et al. [48] predicted geometric structure, vibrational frequencies (harmonic and anharmonic) as well as some energy and thermodynamics characteristics of the strontium, barium, and radium monohydroxides. It should be worth mentioning that the anharmonic corrections in Ref. [48] were obtained from fits to the near-equilibrium potential energy surfaces, or in other words, they do not include the dependence of the bending mode energy levels on the vibrational angular momentum quantum number (*vide infra*). As a result, the anharmonic corrections for the bending mode reduce the harmonic frequency to the anharmonic one from 400.6 to 375.3 cm^{-1} for SrOH, from 379.9 to 363.7 cm^{-1} for BaOH, and from 378.7 to 366.5 cm^{-1} for RaOH [48]. On the contrary, the harmonic frequency of the bending mode (347.6 cm^{-1}) for the CaOH radical [49] turns out to be lower than the fundamental one (351.9 cm^{-1}) if the mentioned dependence is taken into account. Gaul and Berger [50] calculated molecular structural parameters and *P*, *T*-violating properties for the ground state of the Ca, Sr, Ba, Ra, and Yb monohydroxides at the GHF-ZORA (generalized Hartree–Fock zeroth-order regular approximation) and GKS-ZORA/B3LYP (generalized Kohn–Sham) levels of theory. According to their calculations, the equilibrium structure of the mentioned radicals is not linear. Up to date, the most accurate calculations of the characteristics of the RaOH ground state were performed by Zakharova and Petrov [51] at the CCSD(T) level of theory. Zakharova and Petrov [51] calculated the 2D potential energy surface (PES) of the RaOH ground state as a function of stretching RaO and bending coordinates, as well as predicted the *P*, *T*-odd parameters and the fundamental frequencies of the stretching RaO and bending modes. When this paper was ready for submission, Zhang et al. [52] published their results on polyatomic linear molecules, including CaOH, SrOH, YbOH, and RaOH. Regarding the latter, Zhang et al. [52] calculated the ground state PES, vibrational levels of the stretching RaO and bending modes, as well as vibrational branching ratios for some transitions for the $\tilde{A}^2\Pi_{1/2} \rightarrow \tilde{X}^2\Sigma^+$ channel.

So, previously most theoretical efforts have been focused on the prediction of parameters of the *P*-, *T*-odd effects and some characteristics of the RaOH ground state. Lately, we performed the state-of-the-art FS-RCCSD (Fock-space relativistic coupled cluster singles and doubles) calculations to obtain spectroscopic properties of the ground and low-lying excited states of heavy metal atom containing diatomics [15, 53–56] including radium monohalides. Herein, we use the same level of theory for the systematic analysis of the properties of the lowest vibronic states of the

radium monohydroxide molecule expecting to achieve the best results for this triatomic radical. Namely, we present an accurate *ab initio* characterization of the potential energy surfaces (PESs), permanent and transition dipoles, vibrational energy levels, Franck–Condon factors, radiative lifetimes and finally evaluate cooling parameters and propose direct laser cooling schemes for the RaOH and RaOD molecules.

2. Computational details

The PESs of the ground and five lowest excited states of the RaOH radical were calculated within the Kramers unrestricted IH-FS-RCCSD (intermediate Hamiltonian Fock-space relativistic coupled cluster singles and doubles) [57, 58] method using the DIRAC19 quantum chemical package [59]. Nowadays, the FS-RCC approach is one of the most successful tools for predicting the electronic structure and properties of the ground and lower excited states of molecular compounds containing heavy atoms. It provides the most accurate data on potential energy curves, PESs, and other characteristics (e.g., ionization potential and electron affinity) of excited states of small molecular systems [60–63]. Its theoretical accuracy for the predicted electronic transition energies and/or dissociation energy limits is evaluated to be less than 100 cm^{-1} for alkaline earth metal monohalides [15, 57, 64–66] and even better for some alkali metal diatomics [55, 67, 68]. However, the problem of intruder states and the lack of convergence for large internuclear distances and asymmetric molecular configurations (e.g., bend configurations of a linear molecule) force one to use the intermediate Hamiltonian approach and limit the calculations to rather small internuclear distances besides the equilibrium molecular configuration. Concerning the alkaline earth metal monohalide type molecules, another limitation of the approximation mentioned above rises from their particular electronic structure. The lowest molecular terms of an MX radical (where M is an alkaline earth metal atom and X is a halide atom or a pseudohalide functional group) have more or less ionic character, although the higher terms are non-bonded covalent ones (see e.g., calculated potential energy curves and surfaces of the RaCl [69] and SrOH [70] radicals), which strongly perturbate the ionic terms at the large internuclear distances. These covalent states cannot be taken into account simultaneously with ionic ones in the framework of the (0*h*, 1*p*) Fock sector used here. For the characteristics of the radium monohalides ground state RCCSD(T) and FS-RCCSD methods give very similar results [15, 53, 54], however, for excited states, the effects of orbital relaxation due to an electron's attachment should be also considered [60, 62]. In the framework of the FS-CC approach, most of the orbital relaxation effects are taken into account by single-electronic excitation amplitudes [60, 63], and the rest part seems to be important rather for the (0*h*, 2*p*) and (1*h*, 1*p*) Fock sectors than for the (0*h*, 1*p*) one [60].

Within the approach mentioned, an effective Hamiltonian is defined in a model space, which is constructed from Slaters determinants. A reference zero-order wave function (or vacuum state) is a closed-shell determinant, and the operator of the excitation is defined relative to the vacuum state and divided into parts according to the number of valence holes and valence electrons. To avoid intruder states and convergence difficulties, the intermediate Hamiltonian (IH) formalism [58] was also used. In the case of alkaline earth metal monohalide or monohydroxide MX radicals, the vacuum state is the closed-shell positively charged ion MX^+ (or 0 holes and 0 electrons over vacuum).

Thus, the first step of calculations is a solution of the coupled cluster equations for a closed-shell reference ion (or (0,0) Fock sector). The final step is adding an electron and solving the coupled cluster equations for an open-shell neutral MX molecule in the (0*h*, 1*p*) Fock sector (0 holes, 1 electron, or 1 particle over vacuum). Calculations were started by generating pseudospinors at the HF-SCF level of theory for the closed-shell ground state of the $RaOH^+$ ion. Then the IH-FS-RCCSD calculations in the (0*h*, 1*p*) Fock sector were performed for the $RaOH^+$ ion for the ground and five lower excited states.

The Stuttgart ECPDS78MDFSO fully relativistic large effective core potential [71] was used for the radium atom. It replaces 78 chemically inactive core electrons with empirical pseudo-potentials, includes the spin-orbit parameters and takes into account the Breit interaction in the computational scheme. The Gaussian all-electron cc-pVTZ [3s2p1d] [72] and cc-pCVTZ [6s5p3d1f] [73] basis sets, and cc-pCVTZ-PP [7s6p5d3f] [74] basis set were used for the hydrogen and oxygen atoms and the remaining radium electrons, respectively. All ten remaining electrons of the radium atom (namely, eight subvalence, or outer core $6s^26p^6$ electrons and two valence $7s^2$ electrons), one 1s electron of the hydrogen atom, and all eight electrons of the oxygen atom ($1s^22s^22p^4$) were included in correlation calculations. The virtual energy cutoff has been set to 1000 E_h. The active space included six Kramers pairs of the lowest spinors arising from the 7s and 6d states of Ra^+ ion. The calculations were performed pointwise for the 1.85–3.35 Å and 0.6–2.00 Å internuclear distances by steps of 0.05 Å along the Ra–O (R) and O–H (r) bonds, respectively, and by step of 5.0° along the Ra–O–H angle (θ) in the 0.0–65.0° region (the linear configuration of the molecule corresponds to $\theta = 0$).

The vibrational levels for each electronic state were calculated within Yurchenko et al. [75, 76] method using the TROVE software [75]. The RaOH as a triatomic linear molecule is characterized by two stretching modes (RaO stretching ν_1 and OH stretching ν_3) and a doubly degenerate bending mode ν_2. The corresponding quantum numbers for vibrational states are (v_1, v_2^l, v_3), where vibrational angular momentum quantum number l takes values $|l| = 0, 2, 4, \ldots, v_2$ for v_2 even, and $|l| = 1, 3, 5, \ldots, v_2$ for v_2 odd [8]. One-dimensional basis functions were numerically generated using the Numerov-Cooley method. The associated Laguerre polynomials were used for the bending mode [75, 76]. The PESs were written as polynomial expansions like those used by Koput and Peterson [49] for the calcium monohydroxide radical. The calculations of the FCFs were performed using the numerical integration of the vibrational functions. Since the equilibrium configurations of the ground and excited states almost coincide (*vide infra*), the Duschinsky transformation is not required.

In so far, as the excitation of the stretching OH mode is not expected to be strongly coupled to either the stretching RaO mode or bending mode [44], we have limited ourselves to the consideration of the following models for each electronic state:

1) 1D + 1D + 1D model, or Model I, which is a system of three non-interacting anharmonic oscillators (stretching RaO, bending, and stretching OH modes). In this case, PESs are just cross-sections of the complete PESs along the corresponding coordinates;
2) 2D + 1D model, or Model II, within which 2D PESs were calculated for interacting stretching RaO and stretching OH modes. The 2D PESs were completed by cross-sections of the complete PESs along the bending mode;
3) another 2D + 1D model, or Model III, within which 2D PESs were calculated for interacting stretching RaO and bending modes. The 2D PESs were completed by cross-sections of the complete PESs along the stretching OH mode.

Based on these models we can evaluate the actual mode coupling and their mutual influence. Since the calculation of the complete 3D PESs usually is a very laborious and costly task, we also can define the most rational way to solve similar problems.

The direct evaluation of electric permanent and transition dipole moments is not implemented in the FS-RCC method. Therefore, these calculations were performed at the COSCI/cc-pCVTZ (complete open shell configuration interaction [77]) level of theory with the same set of the active orbitals using the DIRAC19 quantum chemical package [59].

3. Results and discussion

Some calculated molecular parameters of the lowest PESs of the RaOH radical are listed and compared with previous theoretical studies in Table 1. There are no experimental data for radium monohydroxide molecule. Nevertheless, our earlier calculations [15] within the same approach for the RaF molecule demonstrated agreement with the available experimental data [14, 78] and the adequacy of the chosen calculation model.

Table 1. Calculated molecular parameters for the RaOH molecule.

State	T_e, cm^{-1}	R_e (Ra–O), Å	θ, deg	r_e (O–H), Å	D, a.u.
$\tilde{X}^2\Sigma^+$	0.0	2.297 [a)] 2.38 [b)] 2.30 [c, d)] 2.306 [e)] 2.315 [f)] 2.289 [g)] 2.33 [h)] 2.274 [i)]	0.0 [a, b, c, d, e, h, i)] 0.07 [f, g)]	0.951 [a)] 0.94 [b)] 0.957 [e)] 0.935 [f)] 0.956 [g)] 0.969 [h)] 0.952 [i)]	0.46 [a)] 0.82 [b)]
$\tilde{A}^2\Pi_{1/2}$	12 711.3 [a)] 12 000 [b)] 13 800 [c)] 12 600 [d)]	2.289 [a)] 2.35 [b)] 2.29 [c, d)]	0.0 [a, b, c, d)]	0.951 [a)] 0.94 [b)]	1.01 [a)] 0.67 [b)]
$\tilde{A}^2\Pi_{3/2}$	14 625.5 [a)]	2.284 [a)]	0.0 [a)]	0.951 [a)]	0.99 [a)]
$\tilde{B}^2\Delta_{3/2}$	15 239.8 [a)]	2.304 [a)]	0.0 [a)]	0.950 [a)]	2.21 [a)]
$\tilde{C}^2\Sigma^+$	15 616.0 [a)]	2.297 [a)]	0.0 [a)]	0.951 [a)]	1.98 [a)]
$\tilde{B}^2\Delta_{5/2}$	15 847.0 [a)]	2.300 [a)]	0.0 [a)]	0.950 [a)]	2.21 [a)]

Notes:
[a)] this study;
[b)] [16], ARECP/MCSCF;
[c)] [16], SF/FS-RCCSD;
[d)] [16], DC/FS-RCCSD;
[e)] [48], CCSD(T)/aug-cc-pwCVTZ;
[f)] [50], ZORA/cGHF;
[g)] [50], ZORA/cGKS/B3LYP;
[h)] [51], CCSD(T)/GRECP/cc-pVTZ;
[i)] [52], SFX2C-1e-EOMEA-CCSD/ANO-RCC/cc-pVTZ.

Since RaF is isoelectronic with RaOH, it can be assumed that their electronic states will be similar. A comparison of the electronic states of both molecules is given in Fig. 1. The calculations were performed at the FS-RCCSD/cc-pCVTZ (RaF [15]) and IH-FS-RCCSD/cc-pCVTZ (RaOH) levels of theory. The main differences between the two systems of states are the positions of the $B^2\Delta_{3/2}$ ($\tilde{B}^2\Delta_{3/2}$) and $C^2\Sigma^+$ ($\tilde{C}^2\Sigma^+$) terms. For the RaF radical, the $B^2\Delta_{3/2}$ term lies between components of the $A^2\Pi$ state and the $C^2\Sigma^+$ is over the $B^2\Delta_{5/2}$ term. For the RaOH radical the $\tilde{B}^2\Delta_{3/2}$ term is over the $\tilde{A}^2\Pi_{3/2}$ state and the $\tilde{C}^2\Sigma^+$ lies between components of the $\tilde{B}^2\Delta$ term. The spin-orbit splitting of the $A^2\Pi$ ($\tilde{A}^2\Pi$) state for both molecules is similar: 2067/2034 cm^{-1} (RaF, experimental [14]/theoretical [15]) and 1914 cm^{-1} (RaOH), and agrees with the spin-orbit splitting of the first excited ^2D state of the Ra^+ ion (1659 cm^{-1} [79]). The spin-orbit splitting of the $B^2\Delta$ ($\tilde{B}^2\Delta$) term is 762 cm^{-1} (RaF [15]) and 607 cm^{-1} (RaOH).

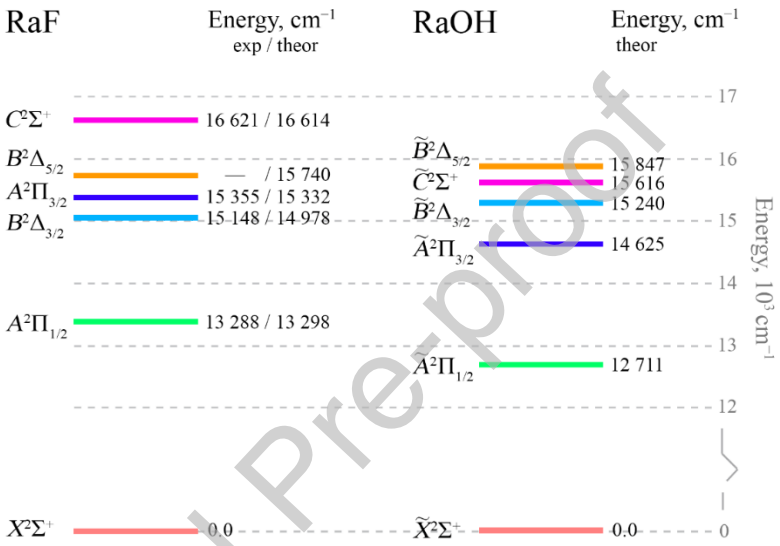

Fig. 1. A comparison of the electronic states of isoelectronic RaF (experimental [14]/theoretical at the FS-RCCSD/cc-pCVTZ level of theory [15]) and RaOH (theoretical at the IH-FS-RCCSD/cc-pCVTZ level of theory) molecules.

Calculated 1D and 2D PESs are shown in Figs 2 and 3. Calculations confirmed the linearity of the molecule not only in the ground state, but also in the lower excited electronic states, as well as the pronounced ionic character of the Ra–OH bonding. It also follows from the structure of molecular orbitals shown in Fig. 4, which demonstrates the concentration of the electronic density mainly on the radium atom in the highest occupied and lowest unoccupied orbitals. The molecular orbitals were generated at the HF level of theory and visualized using the Avogadro software [80]. The isosurface cutoff value was 2×10^{-7}. As a result, the equilibrium length of the Ra–O bond is almost the same in the ground state (2.297 Å) and lower excited $\tilde{A}^2\Pi_{1/2}$ (2.289 Å) and $\tilde{A}^2\Pi_{3/2}$ (2.284 Å) states.

Radium has no stable isotopes; the longest-lived isotope of radium is ^{226}Ra with a half-life of about 1600 years. Oxygen has three stable isotopes (^{16}O, ^{17}O, and ^{18}O) with abundances of 99.8 %, < 0.1 %, and 0.2 %, respectively. We calculated the vibrational energies for the radium monohydroxide radicals ($^{226}Ra^{16}OH$ and $^{226}Ra^{16}OD$), which include the most stable isotope of radium (m_{Ra} = 226.0254 Da), the most abundance isotope of oxygen (m_O = 15.99491 Da) as well as protium (m_H = 1.007825 Da) and deuterium (m_D = 2.014102 Da), for six low-lying electronic states

and then obtained the harmonic vibrational frequencies and other molecular spectroscopic parameters for these states. Calculated vibrational energies and zero point energies (ZPE) for all models under consideration are given in Tables 2–4 and S1–S3 (see Supplementary Material).

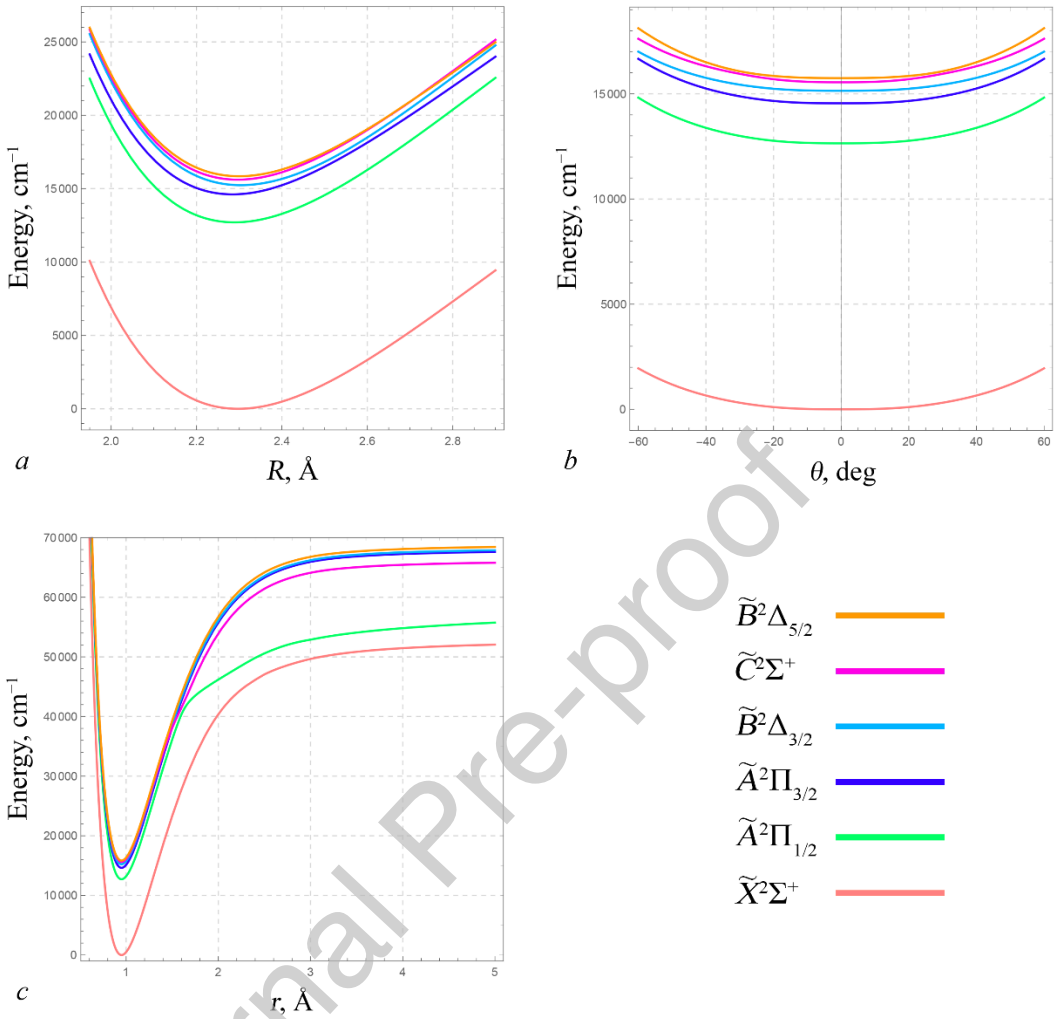

Fig. 2. Cross-sections of the PESs of the RaOH molecule along Ra–O (*a*) bond, Ra–O–H angle (*b*), and O–H bond (*c*).

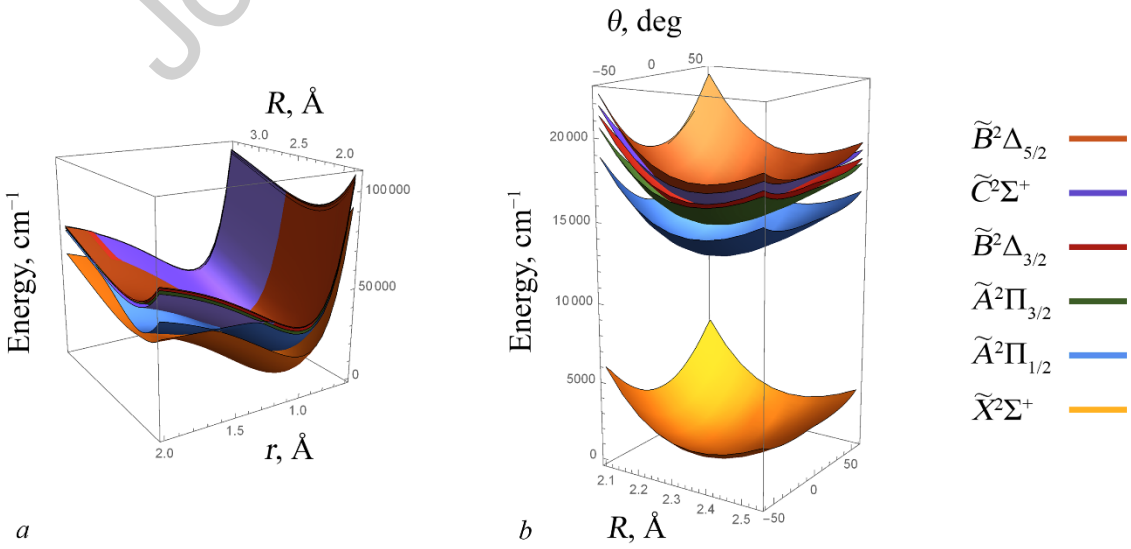

Fig. 3. 2D PESs of the RaOH molecule as functions of (*R*, *r*) (*a*) and (*R*, *θ*) (*b*).

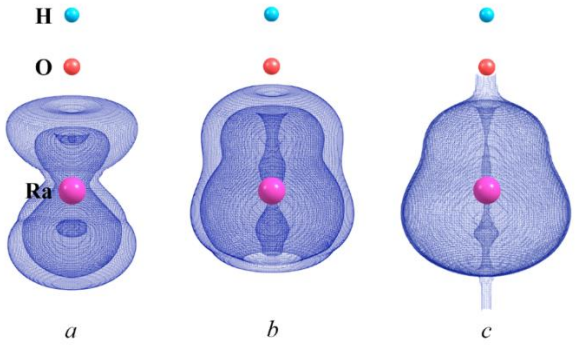

Fig. 4. Isosurfaces of the highest occupied (*a*) and two lowest unoccupied (*b*, *c*) orbitals of the RaOH molecule.

Table 2. Calculated vibrational energies (cm^{-1}) for the ground $\tilde{X}^2\Sigma^+$ state.

$v_1 v_2^l v_3$	$^{226}Ra^{16}OH$			RaOH [a]	$^{226}Ra^{16}OD$		
	Model I	Model II	Model III	[52]	Model I	Model II	Model III
00^00	0	0	0	0	0	0	0
10^00	468	468	478	475	458	459	471
20^00	934	934	953	947	913	914	938
30^00	1396	1396	1425	—	1366	1363	1399
01^10	331	331	326	337	231	231	232
02^00	640	641	632	646	434	434	440
02^20	671	671	663	678	470	470	476
03^10	950	950	948	—	655	655	661
03^30	1017	1017	1009	—	716	716	732
00^01	3824	3820	3824	—	2821	2817	2822
00^02	7488	7481	7487	—	5555	5548	5558
ZPE	2538	2537	2539	—	1904	1903	1911

Note:
[a] unknown isotopes.

Table 3. Calculated vibrational energies (cm^{-1}) for the first excited $\tilde{A}^2\Pi_{1/2}$ state.

$v_1 v_2^l v_3$	$^{226}Ra^{16}OH$			$^{226}Ra^{16}OD$		
	Model I	Model II	Model III	Model I	Model II	Model III
00^00	0	0	0	0	0	0
10^00	476	476	483	451	452	464
20^00	948	948	963	900	900	925
30^00	1417	1417	1440	1346	1345	1383
01^10	350	350	348	233	233	234
02^00	679	679	676	431	431	437
02^20	709	709	707	467	467	472
03^10	1004	1003	1016	632	633	643
03^30	1073	1073	1078	698	698	713
00^01	3833	3826	3836	2828	2821	2829
00^02	7501	7492	7511	5567	5556	5569
ZPE	2566	2561	2568	1916	1910	1923

Table 4. Calculated vibrational energies (cm^{-1}) for the second excited $\tilde{A}^2\Pi_{3/2}$ state.

$v_1 v_2^l v_3$	$^{226}Ra^{16}OH$			$^{226}Ra^{16}OD$		
	Model I	Model II	Model III	Model I	Model II	Model III
00^00	0	0	0	0	0	0
10^00	473	475	483	460	461	475
20^00	942	945	960	917	919	946
30^00	1407	1410	1431	1372	1374	1415
01^10	342	342	344	227	227	229
02^00	662	662	669	422	422	432
02^20	692	692	700	455	455	464
03^10	977	977	1005	617	618	640
03^30	1047	1047	1067	680	681	703
00^01	3832	3828	3832	2826	2821	2826
00^02	7504	7498	7505	5567	5557	5568
ZPE	2554	2553	2564	1910	1908	1917

These results show that the coupling of stretching modes is actually very weak (Model II). For the ground state in fact, it just reduces the levels of the stretching OH mode by 0.1 % (or 4 cm^{-1} for the (00^01) state) and does not affect the levels of the stretching RaO one. The same trend is observed for the excited $\tilde{A}^2\Pi_{1/2}$ state. For the other excited states, the coupling between stretching modes manifests in weak increasing or decreasing of the states of the stretching RaO mode.

In contrast, within the Model III the coupling between the stretching RaO and bending modes is observed. It results in increasing the states of the stretching RaO mode by 2 % and decreasing (as a rule) the states of the bending mode by 1–2 %.

Calculated harmonic and fundamental frequencies as well as anharmonic constants for the lowest states of the RaOH and RaOD molecules are listed and compared with previous theoretical studies in Tables 5 and S4–S6. Vibrational parameters were obtained using the equation

$$E(v_1, v_2, l, v_3) = \omega_1\left(v_1 + \tfrac{1}{2}\right) + x_{11}\left(v_1 + \tfrac{1}{2}\right)^2 + \omega_2(v_2 + 1) + x_{22}(v_2 + 1)^2 + g_{22}l^2$$
$$+\omega_3\left(v_3 + \tfrac{1}{2}\right) + x_{33}\left(v_3 + \tfrac{1}{2}\right)^2$$
$$+x_{12}\left(v_1 + \tfrac{1}{2}\right)(v_2 + 1) + x_{13}\left(v_1 + \tfrac{1}{2}\right)\left(v_3 + \tfrac{1}{2}\right) + x_{23}(v_2 + 1)\left(v_3 + \tfrac{1}{2}\right),$$

where $x_{12} = x_{13} = x_{23} = 0$ for the Model I, $x_{12} = x_{23} = 0$ for the Model II, and $x_{13} = x_{23} = 0$ for the Model III. The values of the harmonic frequencies for the bending mode were determined using the lowest vibrational fundamental, overtone, and combinational levels including ones with $l \neq 0$.

Taking into account the interaction between the stretching RaO and bending modes redistributes the anharmonicity between the $x_{22}(v_2 + 1)^2$ and $g_{22}l^2$ terms (see Tables S5 and S6). For the RaOH radical the contribution of the "pure" vibrational anharmonicity constant x_{22} reduces from 3.35 cm^{-1} (Model I) to 2.68 cm^{-1} (Model III) while the contribution of the "angular" anharmonicity constant g increases from 7.53 cm^{-1} (Model I) to 7.70 cm^{-1} (Model III).

Our predicted fundamental frequencies for the ground state are 478 cm^{-1} (stretching RaO mode), 326 cm^{-1} (bending mode), and 3821 cm^{-1} (stretching OH mode). The first two of them are comparable with Zhang et al. [52] data (475 and 337 cm^{-1}).

Table 5. Calculated harmonic and fundamental frequencies (cm^{-1}) of the $^{226}Ra^{16}OH$ molecule.

State	Stretching ν_1 mode		Bending ν_2 mode		Stretching ν_3 mode	
	Harmonic frequency	Fundamental frequency	Harmonic frequency	Fundamental frequency	Harmonic frequency	Fundamental frequency
$\tilde{X}^2\Sigma^+$	472 [a]	468 [a]	334 [a]	331 [a]	3985 [a]	3824 [a]
	472 [b]	468 [b]	334 [b]	331 [b]	3983 [b]	3821 [b]
	486 [c]	478 [c]	329 [c]	326 [c]	3985 [c]	3824 [c]
	437 [d]		366 [d]		4243 [d]	
	461.5 [e]	451.6 [e]	378.7 [e]	366.5 [e]	3903.7 [e]	3733.7 [e]
	469 [f]		363 [f]			
		475 [g]		337 [g]		
$\tilde{A}^2\Pi_{1/2}$	479 [a]	476 [a]	353 [a]	350 [a]	3998 [a]	3833 [a]
	479 [b]	476 [b]	353 [b]	350 [b]	3987 [b]	3826 [b]
	492 [c]	483 [c]	349 [c]	348 [c]	3997 [c]	3836 [c]
	461 [d]		383 [d]		4248 [d]	
$\tilde{A}^2\Pi_{3/2}$	477 [a]	473 [a]	343 [a]	342 [a]	3991 [a]	3832 [a]
	480 [b]	475 [b]	343 [b]	342 [b]	3986 [b]	3828 [b]
	495 [c]	483 [c]	346 [c]	344 [c]	3992 [c]	3832 [c]
$\tilde{B}^2\Delta_{3/2}$	468 [a]	466 [a]	325 [a]	317 [a]	3992 [a]	3831 [a]
	465 [b]	463 [b]	325 [b]	318 [b]	3964 [b]	3828 [b]
	490 [c]	482 [c]	322 [c]	317 [c]	3991 [c]	3830 [c]
$\tilde{C}^2\Sigma^+$	476 [a]	473 [a]	392 [a]	363 [a]	3980 [a]	3816 [a]
	476 [b]	468 [b]	392 [b]	363 [b]	3980 [b]	3814 [b]
	489 [c]	474 [c]	385 [c]	360 [c]	3981 [c]	3817 [c]
$\tilde{B}^2\Delta_{5/2}$	468 [a]	465 [a]	324 [a]	316 [a]	3991 [a]	3830 [a]
	468 [b]	464 [b]	324 [b]	316 [b]	3987 [b]	3826 [b]
	484 [c]	475 [c]	320 [c]	313 [c]	3991 [c]	3830 [c]

Notes:
[a] this study, Model I;
[b] this study, Model II;
[c] this study, Model III;
[d] [16], ARECP/MCSCF;
[e] [48], CCSD(T)/aug-cc-pwCVTZ;
[f] [51], CCSD(T)/GRECP/cc-pVTZ;
[g] [52], SFX2C-1e-EOMEA-CCSD/ANO-RCC/cc-pVTZ.

The accuracy of our predicted frequency of the stretching RaO mode can be evaluated according to Kinsey-Nielsen et al. [34] assumption. Considering linear alkaline earth metal monohydroxides (CaOH, SrOH, and BaOH), Kinsey-Nielsen et al. [34] noted that as the mass of the metal (M) increases the MO stretching frequency decreases. Treating the hydroxyl group as a single mass, the observed MO frequency (609.0 cm^{-1} for CaOH [19], 527.0 cm^{-1} for SrOH [30], and 492.4 cm^{-1} for BaOH [34]) linearly depends on the square root of the reciprocal of the metal–hydroxyl reduced mass [34]. Extrapolation of this dependence on the RaOH molecule results in the frequency of the RaO mode of 475.7 cm^{-1}, which is consistent with both of our predicted values (468 cm^{-1} for the Model II and 478 cm^{-1} for the Model III). Zakharova and Petrov [51] and Zhang et al. [52] predict 469 and 475 cm^{-1} for the stretching RaO mode, respectively.

Regarding the bending mode, the splitting between the (02^20) and (02^00) levels for the RaOH is predicted to be equal 31 cm^{-1}, which agrees with the experimental data for CaOH (24.4 cm^{-1} [19]) and SrOH (30.2 cm^{-1} [30]) radicals, and predicted value for similar molecule YbOH (24 cm^{-1} [44]). The vibrational constant g_{22} for the ground state is predicted to be 7.7 cm^{-1} for the RaOH radical that also agrees with the data obtained for the CaOH (7.53 cm^{-1} [22]), CaOD (4.37 cm^{-1} [22]), SrOH (7.56 cm^{-1} [28]), and YbOH (5 cm^{-1} [44]) molecules.

Concerning the stretching OH mode, it is worth mentioning that in fact there is only one measurement of this mode for all alkaline earth metal monohydroxides family. Usually due to high frequency, the OH mode is not likely to be populated under the conditions of the experiment (namely, laser induced fluorescence) [35, 36] and is not observed. Pereira and Levy [23] report its frequency is 3778/2790 cm^{-1} in CaOH/CaOD. Note that Jarman and Bernath [17] also give values of 3847 ± 10 cm^{-1} for CaOH and 3766 ± 10 cm^{-1} for SrOH, however, they refer to the unpublished results. The most accurately calculated values based on PES model are 3793/2800 cm^{-1} for CaOH/CaOD [49], 3851/2846 cm^{-1} for MgOH/MgOD [81] and 3865/2855 cm^{-1} for BeOH/BeOD [82]. So, our predicted frequency of 3821/2817 cm^{-1} (RaOH/RaOD) does not contradict the mentioned data and evaluations.

The experiment on direct laser cooling of a linear triatomic molecule (SrOH [12], CaOH [10], and YbOH [13]) usually includes vibrational levels (00^00), (10^00), (20^00), (01^10), (02^00), and (02^20) of the ground $\tilde{X}^2\Sigma^+$ state and the lowest vibrational levels of the first excited $\tilde{A}^2\Pi_{1/2}$ (SrOH [12], CaOH [10], and YbOH [13]) and $\tilde{B}^2\Sigma^+$ (SrOH [12] and CaOH [10]) states to provide cooling, cleaning-up and detection of molecules. So, we focused on radiative properties of the lowest vibrational levels of the $\tilde{A}^2\Pi_{1/2}$ and $\tilde{A}^2\Pi_{3/2}$ states of the RaOH and RaOD molecules. Based on the calculated PESs and vibrational energies, we predicted the Franck–Condon factors and vibrational branching ratios (VBRs), which, in contrast to FCFs, can be directly measured in a spectroscopic experiment. The VBRs were evaluated by the following equation:

$$b_{v'v''} = \frac{f_{v'v''}(\Delta E_{v'v''})^3}{\sum_k f_{v'k}\,(\Delta E_{v'k})^3},$$

where v' and v'' are numbers of upper and lower vibrational levels; $f_{v'v''}$, and $\Delta E_{v'v''}$ are the FCF and the energy difference between v' and v'' states, respectively.

Calculated FCFs for the stretching modes, bending mode and total FCFs are given in Tables 6, 7, S7, and S8. The FCFs for the stretching modes include factor for the OH mode. Our predicted FCF for the $\tilde{A}^2\Pi_{1/2}(00^00) \rightarrow \tilde{X}^2\Sigma^+(00^00)$ is 0.998611 (Model III) that significantly exceeds Isaev et al. [16] values (0.9050/MCSCF, 0.9470/FS-RCCSD/RCC-ANO basis, and 0.9566/FS-RCCSD/Dyall's basis) based on the RaX (where X = OH) pseudomolecule model. Our calculated VBRs for the 0_0^0, 1_1^0, 1_2^0, and 2_2^0 transitions (99.882, 0.007, 0.002, and 0.113 %) consistent with Zhang et al. [52] predicted values (98.972, 0.863, 0.012, and 0.138 %).

Transition dipole moments (TDMs) for the $\tilde{A}^2\Pi_{1/2} \rightarrow \tilde{X}^2\Sigma^+$ and $\tilde{A}^2\Pi_{3/2} \rightarrow \tilde{X}^2\Sigma^+$ transitions are predicted to be 1.988 and 1.901 a.u., respectively. Based on the calculated TDMs, FCFs, and vibrational levels, the lifetimes $\tau_{v'}$ (in seconds) of vibrational levels v' were estimated according to the following equation:

$$\tau_{v'} = \frac{1}{A_{v'}} = \frac{4.936 \times 10^5}{|\mathrm{TDM}|^2 \sum_{v''} f_{v'v''}\,(\Delta E_{v'v''})^3},$$

where $A_{v'}$ is the Einstein coefficient for spontaneous emission.

The predicted radiative lifetimes of the (00^00), (10^00), (20^00), (01^10), (02^00), and (02^20) levels of the excited $\tilde{A}^2\Pi_{1/2}$ and $\tilde{A}^2\Pi_{3/2}$ states are about 60 and 43 ns, respectively. The corresponding

Einstein coefficients are $1.66 \cdot 10^7$ and $2.30 \cdot 10^7$ 1/s, respectively. The calculated lifetimes are consistent with our predicted ones for the radium monohalides [15, 53, 54, 56] and the upper experimental limit (≤ 50 ns) for the $A^2\Pi_{1/2}$ ($v = 0$) state of the radium monofluoride [14]. Isaev et al. [16] report $\tau_0 \approx 40$ ns for the $\tilde{A}^2\Pi_{1/2}(00^00)$ state of the RaOH molecule.

Table 6. Calculated FCFs and VBRs for the $\tilde{A}^2\Pi_{1/2}(v_1 v_2^l v_3) \rightarrow \tilde{X}^2\Sigma^+(v_1 v_2^l v_3)$ band of the $^{226}Ra^{16}OH$ molecule.

Upper state	Lower state	Model I				Model II				Model III			
		FCF			VBR	FCF			VBR	FCF			VBR
		Stretching modes [a]	Bending mode	Total		Stretching modes [b]	Bending mode	Total		Stretching modes [c]	Bending mode	Total	
00^00	00^00	0.999972	0.999210	0.999182	0.999305	0.999973	0.999210	0.999183	0.999306	0.999891	0.998720	0.998611	0.998820
00^00	10^00	$<10^{-6}$	0.999210	$<10^{-6}$	$<10^{-6}$	$<10^{-6}$	0.999210	$<10^{-6}$	$<10^{-6}$	0.000077	0.998720	0.000077	0.000069
00^00	20^00	0.000026	0.999210	0.000026	0.000021	0.000025	0.999210	0.000025	0.000020	0.000030	0.998720	0.000030	0.000023
10^00	00^00	$<10^{-6}$	0.999210	$<10^{-6}$	$<10^{-6}$	$<10^{-6}$	0.999210	$<10^{-6}$	$<10^{-6}$	0.000076	0.998720	0.000076	0.000085
10^00	10^00	0.999917	0.999210	0.999127	0.999996	0.999919	0.999210	0.999130	0.999996	0.999700	0.998720	0.998420	0.999795
10^00	20^00	0.000004	0.999210	0.000004	0.000004	0.000004	0.999210	0.000004	0.000003	0.000134	0.998720	0.000134	0.000120
20^00	00^00	0.000026	0.999210	0.000026	0.000032	0.000025	0.999210	0.000025	0.000031	0.000031	0.998720	0.000031	0.000038
20^00	10^00	0.000004	0.999210	0.000004	0.000004	0.000004	0.999210	0.000004	0.000004	0.000130	0.998720	0.000130	0.000145
20^00	20^00	0.999804	0.999210	0.999014	0.999964	0.999809	0.999210	0.999019	0.999965	0.999494	0.998720	0.998215	0.999816
00^00	02^00	0.999972	0.000787	0.000787	0.000674	0.999973	0.000787	0.000787	0.000674	0.999891	0.001278	0.001278	0.001132
01^10	01^10	0.999972	0.998388	0.998360	0.998360	0.999973	0.998388	0.998361	0.998361	0.999891	0.997594	0.997485	0.997485
02^00	00^00	0.999972	0.000789	0.000789	0.000916	0.999973	0.000789	0.000789	0.000875	0.999891	0.001317	0.001317	0.001452
02^00	02^00	0.999972	0.996343	0.996315	0.999060	0.999973	0.996343	0.996316	0.999101	0.999891	0.994338	0.994230	0.998522
02^20	02^20	0.999972	0.996960	0.996932	0.996932	0.999973	0.996960	0.996934	0.996934	0.999891	0.994564	0.994456	0.994456

Notes:
[a] FCFs include the FCF = 0.999999 for the stretching OH mode;
[b] FCFs include the FCF = 1.000000 for the stretching OH mode;
[c] FCFs include the FCF = 0.999999 for the stretching OH mode.

Table 7. Calculated FCFs and VBRs for the $\tilde{A}^2\Pi_{3/2}(v_1 v_2^l v_3) \rightarrow \tilde{X}^2\Sigma^+(v_1 v_2^l v_3)$ band of the $^{226}Ra^{16}OH$ molecule.

Upper state	Lower state	Model I				Model II				Model III			
		FCF			VBR	FCF			VBR	FCF			VBR
		Stretching modes [a]	Bending mode	Total		Stretching modes [b]	Bending mode	Total		Stretching modes [c]	Bending mode	Total	
00^00	00^00	0.999975	0.999765	0.999740	0.999776	0.999974	0.999765	0.999739	0.999777	0.999815	0.999182	0.998997	0.999131
00^00	10^00	0.000009	0.999765	0.000009	0.000008	$<10^{-6}$	0.999765	$<10^{-6}$	$<10^{-6}$	0.000148	0.999182	0.000148	0.000134
00^00	20^00	0.000013	0.999765	0.000013	0.000011	0.000022	0.999765	0.000022	0.000018	0.000034	0.999182	0.000034	0.000027
10^00	00^00	0.000009	0.999765	0.000009	0.000010	$<10^{-6}$	0.999765	$<10^{-6}$	$<10^{-6}$	0.000145	0.999182	0.000145	0.000160
10^00	10^00	0.999875	0.999765	0.999640	0.999922	0.999931	0.999765	0.999696	0.999993	0.999361	0.999182	0.998544	0.999470
10^00	20^00	0.000075	0.999765	0.000075	0.000068	0.000008	0.999765	0.000008	0.000007	0.000409	0.999182	0.000409	0.000370
20^00	00^00	0.000013	0.999765	0.000013	0.000016	0.000022	0.999765	0.000022	0.000026	0.000036	0.999182	0.000036	0.000044
20^00	10^00	0.000073	0.999765	0.000073	0.000080	0.000008	0.999765	0.000008	0.000008	0.000394	0.999182	0.000394	0.000434
20^00	20^00	0.999580	0.999765	0.999345	0.999904	0.999805	0.999765	0.999570	0.999966	0.998590	0.999182	0.997773	0.999522
00^00	02^00	0.999975	0.000234	0.000234	0.000205	0.999974	0.000234	0.000234	0.000205	0.999815	0.000816	0.000816	0.000696
01^10	01^10	0.999975	0.999520	0.999495	0.999495	0.999974	0.999520	0.999494	0.999494	0.999815	0.998489	0.998304	0.998304
02^00	00^00	0.999975	0.000234	0.000234	0.000266	0.999974	0.000234	0.000234	0.000267	0.999815	0.000788	0.000788	0.000897
02^00	02^00	0.999975	0.999069	0.999044	0.999721	0.999974	0.999069	0.999042	0.999713	0.999815	0.996442	0.996258	0.999025
02^20	02^20	0.999975	0.999406	0.999381	0.999381	0.999974	0.999406	0.999380	0.999380	0.999815	0.996358	0.996174	0.996174

Notes:
[a] FCFs include the FCF = 0.999999 for the stretching OH mode;
[b] FCFs include the FCF = 0.999998 for the stretching OH mode;
[c] FCFs include the FCF = 0.999999 for the stretching OH mode.

According to our calculations, the total FCF for the $\tilde{A}^2\Pi_{1/2}(00^00) \rightarrow \tilde{X}^2\Sigma^+(00^00)$ transition (0.998611, Model III) for the RaOH molecule can provide only about 720 scattering photons, which is not enough for the realization of the closed optical scheme for direct laser cooling. The inclusion of additional $(00^00) \rightarrow (02^00)$ (FCF = 0.001278), $(00^00) \rightarrow (10^00)$ (FCF = 0.000077), and $(00^00) \rightarrow (20^00)$ (FCF = 0.000030) cooling channels increases the number of scattered photons up to 250 000. It could provide the complete probability for the molecule being cooled to remain in the cooling loop close to unity (the sum of total FCFs is 0.999996) and realize a quasi-closed optical four-colour laser scheme. The $\tilde{A}^2\Pi_{3/2}(00^00) \rightarrow \tilde{X}^2\Sigma^+(v_1v_2^l0)$ channel also requires four lasers to provide the number of scattered photons up to 200 000.

For the RaOD isotopologue the total FCF for the $\tilde{A}^2\Pi_{1/2}(00^00) \rightarrow \tilde{X}^2\Sigma^+(00^00)$ channel equals to 0.998957 that can provide about 960 absorption/emission cycles. The additional $(00^00) \rightarrow (02^00)$ (FCF = 0.000120) and $(00^00) \rightarrow (10^00)$ (FCF = 0.000918) channels increase the number of scattered photons to the required order (200 000). The $\tilde{A}^2\Pi_{3/2}(00^00) \rightarrow \tilde{X}^2\Sigma^+(v_1v_2^l0)$ transition allows scattering about 110 000 photons using a three-colour laser scheme.

The upper limits for the cooling parameters were evaluated using the following equations

$$T_D = \frac{-h\Gamma^2}{16\pi k_B \Delta}\left(1 + \frac{I}{I_s} + \frac{4\Delta^2}{\Gamma^2}\right), \qquad T_D^{min} = \frac{h\Gamma}{4\pi k_B}, \qquad T_r = \frac{h^2}{Mk_B\lambda^2},$$

where T_D is the Doppler temperature, or the minimum temperature, which can be achieved by the Doppler cooling; h is the Planck's constant; Γ is a natural linewidth, which is related to a radiative lifetime ($\Gamma = 1/\tau$); k_B is the Boltzmann's constant; Δ is a detuning parameter; I is an intensity of laser beam; $I_s = \pi hc\Gamma/(3\lambda^3)$ is the saturation intensity; c is the speed of light; λ is the laser wavelength; T_D^{min} is the minimal Doppler temperature, or the Doppler limit, under the conditions $\Delta = -\Gamma/2$ and $I << I_s$; T_r is the recoil temperature, or sub-Doppler cooling temperature, which can be reached by using, for example, the Sisyphus method; M is the mass of a molecule.

The Doppler limit T_D^{min} for the $\tilde{A}^2\Pi_{1/2}(00^00) \rightarrow \tilde{X}^2\Sigma^+(00^00)$ transition for the RaOH radical is estimated as 64 μK. If the detuning parameter $\Delta = -\Gamma/2$ and the intensity of laser beam $I = 33$ mW/cm^2 (see, for example, experiment on CaOH laser cooling [11]), the Doppler temperature T_D is evaluated as 1.9 mK. The Doppler temperature T_D strongly depends on the detuning parameter Δ and reaches a minimum at $\Delta \approx -1.5\Gamma$. The optimal choice of the detuning parameter Δ reduces this temperature up to 1.2 mK. The recoil temperature T_r is evaluated as 128 nK. All the mentioned cooling parameters are consistent with our previously predicted ones for radium monohalides [15, 53, 54, 56]. For the $\tilde{A}^2\Pi_{3/2}(00^00) \rightarrow \tilde{X}^2\Sigma^+(00^00)$ channel the cooling parameters are of the same order: $T_D^{min} = 89$ μK, $T_D = 1.5$ mK, $T_D^{opt} = 1.2$ mK, $T_r = 169$ nK. Due to the small differences in masses and energy levels, for the RaOD isotopologue the cooling parameters are almost the same.

Figure 5 shows the vibrational cooling scheme for the RaOH molecule, in which all pumping and repumping transitions are driven through the $\tilde{A}^2\Pi_{1/2}(00^00)$ state. According to our calculations, the scheme provides the required number of scattered photons using one pumping and three repumping lasers with wavelengths that fall into the peak power output (750–850 nm) of the tunable Ti:sapphire laser [83].

The last remarks deal with the evaluation of the Renner–Teller effect and *l*-doubling in the RaOH radical. Considering the dimensionless harmonic Renner–Teller parameter ϵ as a quantitative measure of the coupling of the electronic orbital angular momentum and the vibrational angular momentum, which is associated with the degenerate bending mode, Presunka and Coxon [29] as well as Beardah and Ellis [31] note that for SrOH molecule this parameter is small ($\epsilon = -0.0791$ [29]). For alkaline earth metal monohydroxides, the unpaired electron is located on an orbital of the

metal atom while the bending mode may be considered mainly as a displacement of the hydrogen atom due to the relatively large mass of the metal atom. Therefore, the unpaired electron is not strongly coupled to the dipole moment induced by the bending mode [29, 31]. According to Li and Coxon [22], for the lightest CaOH/CaOD molecule the parameter ϵ is equal to –0.0973/–0.0954. Presunka and Coxon [29] expect $|\epsilon| < 0.0791$ for the BaOH. Fernando et al. [35] note that the Renner–Teller effect complicates the vibronic structure of BaOH spectra, but it has not yet been clearly observed either in the BaOH [36–40] or YbOH [41–46] spectra. So, we assume that for the heavier RaOH/RaOD molecule the Renner–Teller effect should be quite weak. The parameter q_v, which defines the *l*-doubling of the $\tilde{X}^2\Sigma^+(01^10)$ state, depends on the rotational constant, the fundamental frequencies of the MO stretching and bending modes as well as the Coriolis coefficient [8] and includes the harmonic and Coriolis terms. For the CaOH, SrOH, and BaOH molecules this parameter equals to 21.6492, 11.8546, and 9.4932 MHz, respectively [20]. For the RaOH, Zakharova and Petrov [51] predict the value of 7.2335 MHz for the complete parameter q_v that allows one to evaluate its harmonic term (5.6879 MHz) and the Coriolis coefficient (0.2132). Our predicted value for the harmonic term (6.6800 MHz) slightly overestimates the Zakharova and Petrov [51] data. Based on the value of the Coriolis coefficient, our calculated complete parameter q_v is 7.7365 MHz. Generally, this quantity critically depends on the accuracy of calculations of the structure and fundamental frequencies of a molecule.

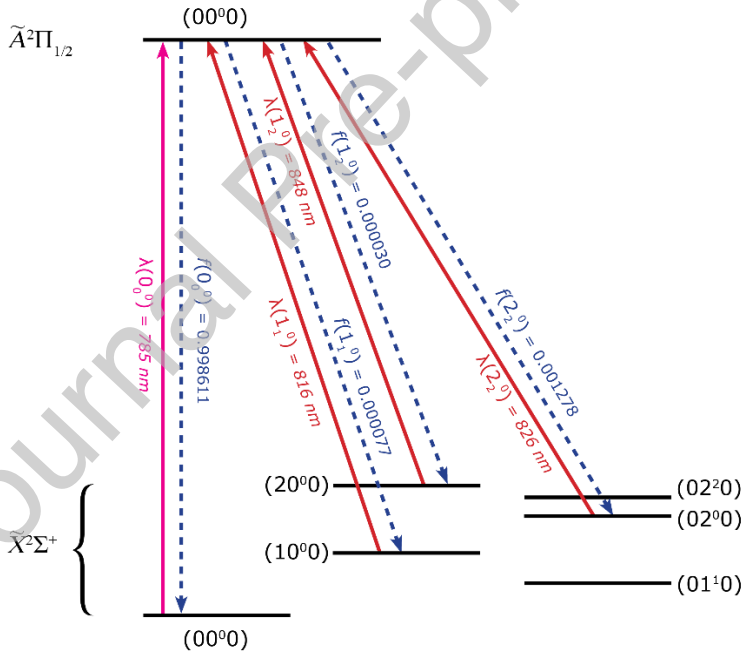

Fig. 5. The vibrational cooling scheme for the RaOH molecule.

4. Conclusion

Based on state-of-the-art quantum chemical calculations at the high level of theory (FS-RCCSD), the detailed molecular spectroscopic parameters of the ground and five lowest excited states of the radium monohydroxide RaOH radical and its deuterated RaOD isotopologue are predicted. The vibrational energy levels and all the fundamental frequencies were calculated for the first time using the potential energy surfaces and taking into account the interaction of the modes. It

was shown that the stretching OH mode is weak coupling with the stretching RaO one and can be considered as a separate non-interacting motion. The FCF for this mode is highly close to unity, however taking into account possible inaccuracies of the calculations, this factor should be considered when the total probability of the laser cooling channels is predicted. The possibilities for the realization of optical cycling schemes for the direct laser cooling involving ground $\tilde{X}^2\Sigma^+$ and first excited $\tilde{A}^2\Pi_{1/2}$ and $\tilde{A}^2\Pi_{3/2}$ states are also considered. The preliminary buffer gas cooling and the use of four-colour laser schemes allow to ensure the fulfillment of the conditions for direct laser cooling and realize a quasi-closed optical cycle for effective cooling of the rarefied radium monohydroxide gas medium.

Declaration of competing interests

The authors declare that they have no known competing financial interests or personal relationships that could have appeared to influence the work reported in this paper.

CRediT authorship contribution statement

Yuliya Osika: Investigation, Formal analysis, Visualization, Writing – original draft, Writing – review & editing. **Sergey Sharashkin:** Investigation, Formal analysis. **George Pitsevich:** Formal analysis, Project administration. **Maksim Shundalau:** Conceptualization, Formal analysis, Investigation, Writing – original draft, Writing – review & editing, Supervision, Project administration.

Acknowledgements

The authors are grateful to Prof. Sergey Yurchenko (Department of Physics and Astronomy, University College London, UK) for his helpful advice and discussions. This work was supported by ATTRACT, a European Union's Horizon 2020 research and innovation project under grant agreement No. 101004462, and the Belarusian State Scientific Research Program "Convergence-2025".

Supplementary Material

Supplementary Material associated with this manuscript can be found in RaOH-SM-revised.docx file.

References

[1] Fitch NJ, Tarbutt MR. Laser-cooled molecules. Adv At Mol Opt Phys 2021;70:157–262. https://doi.org/10.1016/bs.aamop.2021.04.003.

[2] Sunaga A, Abe M, Hada M, Das BP. Merits of heavy-heavy diatomic molecules for electron electric-dipole-moment searches. Phys Rev A 2019;99:062506. https://doi.org/10.1103/PhysRevA.99.062506

[3] Di Rosa MD. Laser-cooling molecules. Concept, candidates, and supporting hyperfine-resolved measurements of rotational lines in the A–X(0,0) band of CaH. Eur Phys J D 2004;31:395–402. https://doi.org/10.1140/epjd/e2004-00167-2

[4] Shuman ES, Barry JF, Glenn DR, DeMille D. Radiative force from optical cycling on a diatomic molecule. Phys Rev Lett 2009;103:223001. http://dx.doi.org/10.1103/PhysRevLett.103.223001

[5] Shuman ES, Barry JF, DeMille D. Laser cooling of a diatomic molecule. Nature 2010;467:820–3. https://doi.org/10.1038/nature09443

[6] Zhelyazkova V, Cournol A, Wall TA, Matsushima A, Hudson JJ, Hinds AE, Tarbutt MR, Sauer BE. Laser cooling and slowing of CaF molecules. Phys Rev A 2014;89:053416. https://doi.org/10.1103/PhysRevA.89.053416

[7] Truppe S, Williams HJ, Hambach M, Caldwell L, Fitch NJ, Hinds EA, Sauer BE, Tarbutt MR. Molecules cooled below the Doppler limit. Nature Phys. 2017;13:1173–6. https://doi.org/10.1038/nphys4241

[8] Herzberg G. Molecular Spectra and Molecular Structure: III. Electronic Spectra and Electronic Structure of Polyatomic Molecules, Reprint Edition, Krieger Publishing Company, 1991.

[9] Hutzler NR. Polyatomic molecules as quantum sensors for fundamental physics. Quantum Sci Technol 2020;5:044011. https://doi.org/10.1088/2058-9565/abb9c5

[10] Baum L, Vilas NB, Hallas C, Augenbraun BL, Raval S, Mitra D, Doyle JM. 1D magneto-optical trap of polyatomic molecules. Phys Rev Lett 2020;124:133201. https://doi.org/10.1103/PhysRevLett.124.133201

[11] Vilas NB, Hallas C, Anderegg L, Robichaud P, Winnicki A, Mitra D, Doyle JM. Magneto-optical trapping and sub-Doppler cooling of a polyatomic molecule. Nature 2022;606:70–4. https://doi.org/10.1038/s41586-022-04620-5

[12] Kozyryev I, Baum L, Matsuda K, Augenbraun BL, Anderegg L, Sedlack AP, Doyle JM. Sisyphus laser cooling of a polyatomic molecule. Phys Rev Lett 2017;118:173201. https://doi.org/10.1103/PhysRevLett.118.173201

[13] Augenbraun BL, Lasner ZD, Frenett A, Sawaoka H, Miller C, Steimle TC, Doyle JM. Laser-cooled polyatomic molecules for improved electron electric dipole moment searches. New J Phys 2020;22:022003. https://doi.org/10.1088/1367-2630/ab687b

[14] Garcia Ruiz RF, Berger R, Billowes J, Binnersley CL, Bissell ML, Breier AA, Brinson AJ, Chrysalidis K, Cocolios TE, Cooper BS, Flanagan KT, Giesen TF, de Groote RP, Franchoo S, Gustafsson FP, Isaev TA, Koszorús Á, Neyens G, Perrett HA, Ricketts CM, Rothe S, Schweikhard L, Vernon AR, Wendt KDA, Wienholtz F, Wilkins SG, Yang XF. Spectroscopy of short-lived radioactive molecules. Nature 202;581:396–400. https://doi.org/10.1038/s41586-020-2299-4

[15] Osika Y, Shundalau M. Fock-space relativistic coupled cluster study on the RaF molecule promising for the laser cooling. Spectrochim Acta A 2022;264:120274. https://doi.org/10.1016/j.saa.2021.120274

[16] Isaev TA, Zaitsevskii AV, Eliav E. Laser-coolable polyatomic molecules with heavy nuclei. J Phys B At Mol Opt Phys 2017;50:225101. https://doi.org/10.1088/1361-6455/aa8f34

[17] Jarman CN, Bernath PF. High resolution laser spectroscopy of the $\tilde{C}^2\Delta$–$\tilde{X}^2\Sigma^+$ transition of CaOH and CaOD: Vibronic coupling and the Renner–Teller effect. J Chem Phys 1992;97:1711–8. https://doi.org/10.1063/1.463158

[18] Li M, Coxon JA. Laser spectroscopy of the CaOH $A^2\Pi$–$X^2\Sigma^+$ (020)–(000) band: Deperturbation of the Fermi resonance, Renner–Teller, and spin–orbit interactions. J Chem Phys 1992;97:8961–9. https://doi.org/10.1063/1.463322

[19] Coxon JA, Li M, Presunka PI. Investigation of excited vibrational levels in the $X^2\Sigma^+$ state of CaOH and CaOD by resolved fluorescence spectroscopy. Mol Phys 1992;76:1463–76. https://doi.org/10.1080/00268979200102231

[20] Fletcher DA, Anderson MA, Barclay WL Jr, Ziurys LM. Millimeter-wave spectroscopy of vibrationally excited ground state alkaline-earth hydroxide radicals ($X^2\Sigma^+$). J Chem Phys 1995;102:4334–9. https://doi.org/10.1063/1.469482

[21] Li M, Coxon JA. High-resolution analysis of the fundamental bending vibrations in the $\tilde{A}^2\Pi$ and $\tilde{X}^2\Sigma^+$ states of CaOH and CaOD: Deperturbation of Renner–Teller, spin–orbit and *K*-type resonance interactions. J Chem Phys 1995;102:2663–74. https://doi.org/10.1063/1.468643

[22] Li M, Coxon JA. Dye laser excitation studies of the $\tilde{A}^2\Pi(100)/(020)$–$\tilde{X}^2\Sigma^+(020)/(000)$ bands of CaOD: Analysis of the $\tilde{A}^2\Pi(100)\sim(020)$ Fermi resonance. J Chem Phys 1996;104:4961–77. https://doi.org/10.1063/1.471762

[23] Pereira R, Levy DH. Observation and spectroscopy of high-lying states of the CaOH radical: Evidence for a bent, covalent state. J Chem Phys 1996;105:9733–9. https://doi.org/10.1063/1.472844

[24] Kozyryev I, Steimle TC, Yu P, Nguyen D-T, Doyle JM. Determination of CaOH and $CaOCH_3$ vibrational branching ratios for direct laser cooling and trapping. New J Phys 2019;21:052002. https://doi.org/10.1088/1367-2630/ab19d7

[25] Zhang C, Augenbraun BL, Lasner ZD, Vilas NB, Doyle JM, Cheng L. Accurate prediction and measurement of vibronic branching ratios for laser cooling linear polyatomic molecules. J Chem Phys 2021;155:091101. https://doi.org/10.1063/5.0063611

[26] Miyamoto Y, Tobaru R, Takahashi Y, Hiramoto A, Iwakuni K, Kuma S, Enomoto K, Baba M. Doppler-free spectroscopy of buffer-gas-cooled calcium monohydroxide. J Phys Chem A 2023;127:4758–63. https://doi.org/10.1021/acs.jpca.2c08565

[27] Brazier CR, Bernath PF. Laser and Fourier transform spectroscopy of the $\tilde{A}^2\Pi$–$\tilde{X}^2\Sigma^+$ transition of SrOH. J Mol Spectrosc 1985;114:163–73. https://doi.org/10.1016/0022-2852(85)90345-5

[28] Presunka PI, Coxon JA. High-resolution laser spectroscopy of excited bending vibrations ($v_2 \leq 2$) of the $\tilde{B}^2\Sigma^+$ and $\tilde{X}^2\Sigma^+$ electronic states of SrOH: Analysis of *l*-type doubling and *l*-type resonance. Can J Chem 1993;71:1689–705. https://doi.org/10.1139/v93-211

[29] Presunka PI, Coxon JA. Laser spectroscopy of the $\tilde{A}^2\Pi$–$\tilde{X}^2\Sigma^+$ transition of SrOH: Deperturbation analysis of *K*-resonance in the v_2=1 level of the $\tilde{A}^2\Pi$ state. J Chem Phys 1994;101:201–22. https://doi.org/10.1063/1.468171

[30] Presunka PI, Coxon JA. Laser excitation and dispersed fluorescence investigations of the $\tilde{A}^2\Pi$–$\tilde{X}^2\Sigma^+$ system of SrOH. Chem Phys 1995;190:97–111. https://doi.org/10.1016/0301-0104(94)00330-D

[31] Beardah MS, Ellis AM. Observation of several new electronic transitions of the SrOH free radical. J Chem Phys 1999;110:11244–54. https://doi.org/10.1063/1.479065

[32] Nguyen D-T, Steimle TC, Kozyryev I, Huang M, McCoy AB. Fluorescence branching ratios and magnetic tuning of the visible spectrum of SrOH. J Mol Spectrosc 2018;347:7–18. https://doi.org/10.1016/j.jms.2018.02.007

[33] Lasner Z, Lunstad A, Zhang C, Cheng L, Doyle JM. Vibronic branching ratios for nearly closed rapid photon cycling of SrOH. Phys Rev A 2022;106:L020801. https://doi.org/10.1103/PhysRevA.106.L020801

[34] Kinsey-Nielsen S, Brazier CR, Bernath PF. Rotational analysis of the $\tilde{B}^2\Sigma^+$–$\tilde{X}^2\Sigma^+$ transition of BaOH and BaOD. J Chem Phys 1986;84:698–708. https://doi.org/10.1063/1.450566

[35] Fernando WTML, Douay M, Bernath PF. Vibrational analysis of the $\tilde{A}^2\Pi$–$\tilde{X}^2\Sigma^+$ and $\widetilde{A}'^2\Delta$–$\tilde{X}^2\Sigma^+$ transitions of BaOH and BaOD. J Mol Spectrosc 1990;144:344–5l. https://doi.org/10.1016/0022-2852(90)90220-K

[36] Pooley SJ, Beardah MS, Ellis AM. Electronic spectroscopy of the $\tilde{C}$–$\tilde{X}$ and $\widetilde{D}$–$\tilde{X}$ transitions of BaOH. J Electron Spectros Relat Phenomena 1998;97:77–88. https://doi.org/10.1016/S0368-2048(98)00260-6

[37] Wang J-G, Tandy JD, Bernath PF. High-resolution laser excitation spectroscopy of the $\tilde{A}^2\Pi(000)$ – $\tilde{X}^2\Sigma^+(000)$ transition of BaOH. J Mol Spectrosc 2008;252:31–6. https://doi.org/10.1016/j.jms.2008.06.006

[38] Tandy JD, Wang J-G, Bernath PF. High-resolution laser spectroscopy of BaOH and BaOD: Anomalous spin-orbit coupling in the $\tilde{A}^2\Pi$ state. J Mol Spectrosc 2009;255: 63–7. https://doi.org/10.1016/j.jms.2009.03.002

[39] Frey SE, Steimle TC. Optical Stark spectroscopy of the $\tilde{A}^2\Pi_r(000) \leftarrow \tilde{X}^2\Sigma^+(000)$ system of barium monohydroxide, BaOH. Chem Phys Lett 2011;512:21–4. https://doi.org/10.1016/j.cplett.2011.06.070

[40] Tandy JD, Wang J-G, Liévin J, Bernath PF. Investigating the electronic states of BaOH by V-type double resonance spectroscopy and *ab initio* calculations: Further evidence of perturbation from the $\tilde{A}'^2\Delta$ state. J Mol Spectrosc 2011;270:44–50. https://doi.org/10.1016/j.jms.2011.08.009

[41] Melville TC, Coxon JA. The visible laser excitation spectrum of YbOH: The $\tilde{A}^2\Pi$–$\tilde{X}^2\Sigma^+$ transition. J Chem Phys 2001;115:6974–8. https://doi.org/10.1063/1.1404145

[42] Steimle TC, Linton C, Mengesha ET, Bai X, Le AT. Field-free, Stark, and Zeeman spectroscopy of the $\tilde{A}^2\Pi_{1/2}$–$\tilde{X}^2\Sigma^+$ transition of ytterbium monohydroxide. Phys Rev A 2019;100:052509. https://doi.org/10.1103/PhysRevA.100.052509

[43] Coxon JA, Linton C. Re-analysis of the 000 – 000 and 000 – 100 bands in the $\tilde{A}^2\Pi_{1/2}$–$\tilde{X}^2\Sigma^+$ system of YbOH: Revised estimates of the ground state spin-rotation splitting parameters. J Mol Spectrosc 2020;367:111242. https://doi.org/10.1016/j.jms.2019.111242

[44] Mengesha ET, Le AT, Steimle TC, Cheng L, Zhang C, Augenbraun BL, Lasner Z, Doyle J. Branching ratios, radiative lifetimes, and transition dipole moments for YbOH. J Phys Chem A 2020;124:3135–48. https://doi.org/10.1021/acs.jpca.0c00850

[45] Pilgram NH, Jadbabaie A, Zeng Y, Hutzler NR, Steimle TC. Fine and hyperfine interactions in ^{171}YbOH and ^{173}YbOH. J Chem Phys 2021;154:244309. https://doi.org/10.1063/5.0055293

[46] Persinger TD, Han J, Le AT, Steimle TC, Heaven MC. Electronic spectroscopy and ionization potentials for YbOH and $YbOCH_3$. Phys Rev A 2023;107:032810. https://doi.org/10.1103/PhysRevA.107.032810

[47] Fan M, Holliman CA, Shi X, Zhang H, Straus MW, Li X, Buechele SW, Jayich AM. Optical mass spectrometry of cold $RaOH^+$ and $RaOCH_3^+$. Phys Rev Lett 2012;126:023002. https://doi.org/10.1103/PhysRevLett.126.023002

[48] Vasiliu M, Hill JG, Peterson KA, Dixon DA. Structures and heats of formation of simple alkaline earth metal compounds II: Fluorides, chlorides, oxides, and hydroxides for Ba, Sr, and Ra. J Phys Chem A 2018;122:316–27. https://doi.org/10.1021/acs.jpca.7b09056

[49] Koput J, Peterson KA. *Ab initio* potential energy surface and vibrational-rotational energy levels of $X^2\Sigma^+$ CaOH. J Phys Chem A 2002;106:9595–9. https://doi.org/10.1021/jp026283u

[50] Gaul K, Berger R. *Ab initio* study of parity and time-reversal violation in laser-coolable triatomic molecules. Phys Rev A 2020;101:012508. https://doi.org/10.1103/PhysRevA.101.012508

[51] Zakharova A, Petrov A. *P,T*-odd effects for the RaOH molecule in the excited vibrational state. Phys Rev A 2021;103:032819. https://doi.org/10.1103/PhysRevA.103.032819

[52] Zhang C, Hutzler NR, Cheng L. Intensity-borrowing mechanisms pertinent to laser cooling of linear polyatomic molecules. J Chem Theory Comput 2023. https://doi.org/10.1021/acs.jctc.3c00408

[53] Osika Y, Shundalau M. Fock-space relativistic coupled cluster study on the spectroscopic properties of the low-lying states of the radium monobromide RaBr molecule. J Quant Spectrosc Radiat Transfer 2021;276:107947. https://doi.org/10.1016/j.jqsrt.2021.107947

[54] Osika Y, Shundalau M, Han Y-C. *Ab initio* study on the spectroscopic and radiative properties of the low-lying states of the radium monoiodide RaI molecule. J Quant Spectrosc Radiat Transfer 2022;285:108144. https://doi.org/10.1016/j.jqsrt.2022.108144

[55] Shundalau M, Lamberti P. Relativistic *ab initio* study on the spectroscopic and radiative properties of the lowest states and modeling of the optical cycles for the LiFr molecule. J Quant Spectrosc Radiat Transfer 2023;296:108467. https://doi.org/10.1016/j.jqsrt.2022.108467

[56] Osika Y, Shundalau M, Han Y-C. Theoretical insights into the spectroscopic properties and prospects for the direct laser cooling of the radium monohalides. Nonlinear Phenom Complex Syst. Submitted article.

[57] Visscher L, Eliav E, Kaldor U. Formulation and implementation of the relativistic Fock-space coupled cluster method for molecules. J Chem Phys 2001;115:9720–6. https://doi.org/10.1063/1.1415746

[58] Meissner L. Fock-space coupled-cluster method in the intermediate Hamiltonian formulation: Model with singles and doubles. J Chem Phys 1998;108:9227–35. https://doi.org/10.1063/1.476377

[59] DIRAC, a relativistic *ab initio* electronic structure program, Release DIRAC19 (2019), written by A.S.P. Gomes, T. Saue, L. Visscher, H.J.Aa. Jensen, and R. Bast, with contributions from I.A. Aucar, V. Bakken, K.G. Dyall, S. Dubillard, U. Ekström, E. Eliav, T. Enevoldsen, E. Faßhauer, T. Fleig, O. Fossgaard, L. Halbert, E.D. Hedegård, T. Helgaker, B. Helmich-Paris, J. Henriksson, M. Iliaš, Ch.R. Jacob, S. Knecht, S. Komorovský, O. Kullie, J.K. Lærdahl, C.V. Larsen, Y.S. Lee, H.S. Nataraj, M.K. Nayak, P. Norman, G. Olejniczak, J. Olsen, J.M.H. Olsen, Y.C. Park, J.K. Pedersen, M. Pernpointner, R. Di Remigio, K. Ruud, P. Sałek, B. Schimmelpfennig, B. Senjean, A. Shee, J. Sikkema, A.J. Thorvaldsen, J. Thyssen, J. van Stralen, M.L. Vidal, S. Villaume, O. Visser, T. Winther, and S. Yamamoto (available at http://dx.doi.org/10.5281/zenodo.3572669, see also http://www.diracprogram.org).

[60] Infante I, Eliav E, Vilkas MJ, Ishikawa Y, Kaldor U, Visscher L. A Fock space coupled cluster study on the electronic structure of the UO_2, UO^+_2, U^{4+}, and U^{5+} species. J Chem Phys 2007;127:124308. https://doi.org/10.1063/1.2770699

[61] Tecmer P, Gomes ASP, Knecht S, Visscher L. Relativistic Fock-space coupled cluster study of small building blocks of larger uranium complexes. J Chem Phys 2014;141:041107. https://doi.org/10.1063/1.4891801

[62] Tecmer P, González-Espinoza CE. Electron correlation effects of the ThO and ThS molecules in the spinor basis. A relativistic coupled cluster study of ground and excited states properties. Phys Chem Chem Phys 2018;20:23424–32. https://doi.org/10.1039/C8CP00048D
[63] Lu Y, Wang Z, Wang F. Intermediate Hamiltonian Fock-space coupled-cluster theory for excitation energies, double ionization potentials, and double electron attachments with spin–orbit coupling. J Chem Phys 2022;156:114111. https://doi.org/10.1063/5.0076462
[64] Hao Y, Pašteka LF, Visscher L, Aggarwal P, Bethlem HL, Boeschoten A, Borschevsky A, Denis M, Esajas K, Hoekstra S, Jungmann K, Marshall VR, Meijknecht TB, Mooij MC, Timmermans RGE, Touwen A, Ubachs W, Willmann L, Yin Y, Zapara A. High accuracy theoretical investigations of CaF, SrF, and BaF and implications for laser-cooling. J Chem Phys 2019;151:034302. https://doi.org/10.1063/1.5098540
[65] Skripnikov LV. Approaching meV level for transition energies in the radium monofluoride molecule RaF and radium cation Ra^+ by including quantum-electrodynamics effects. J Chem Phys 2021;154:201101. https://doi.org/10.1063/5.0053659
[66] Isaev TA, Zaitsevskii AV, Oleynichenko A, Eliav E, Breier AA, Giesen TF, Garcia Ruiz RF, Berger R. *Ab initio* study and assignment of electronic states in molecular RaCl. J Quant Spectrosc Radiat Transfer 2021;269:107649. https://doi.org/10.1016/j.jqsrt.2021.107649
[67] Musiał M, Kucharski SA. First principle calculations of the potential energy curves for electronic states of the lithium dimer. J Chem Theory Comput 2014;10:1200−11. https://doi.org/10.1021/ct401076e
[68] Musiał M, Kucharski SA, Bewicz A, Skupin P, Tomanek M. Electronic states of NaLi molecule: Benchmark results with Fock space coupled cluster approach. J Chem Phys 2021;154:054109. https://doi.org/10.1063/5.0037441
[69] Osika Y, Shundalau M. Multi-reference perturbation theory study on the RaCl molecule promising for the laser cooling. Comp Theor Chem 2020;1188:112972. https://doi.org/10.1016/j.comptc.2020.112972
[70] Li M, Kłos J, Petrov A, Kotochigova S. Emulating optical cycling centers in polyatomic molecules. Commun Phys 2019;2:148. https://doi.org/10.1038/s42005-019-0245-2
[71] Lim IS, Stoll H, Schwerdtfeger P. Relativistic small-core energy-consistent pseudopotentials for the alkaline-earth elements from Ca to Ra. J Chem Phys 2006;124:034107. https://doi.org/10.1063/1.2148945
[72] Dunning TH, Jr. Gaussian basis sets for use in correlated molecular calculations. I. The atoms boron through neon and hydrogen. J Chem Phys 1989;90:1007–23. https://doi.org/10.1063/1.456153
[73] Woon DE, Dunning TH, Jr. Gaussian basis sets for use in correlated molecular calculations. V. Core-valence basis sets for boron through neon. J Chem Phys 1995;103:4572–85. https://doi.org/10.1063/1.470645
[74] Hill JG, Peterson KA. Gaussian basis sets for use in correlated molecular calculations. XI. Pseudopotential-based and all-electron relativistic basis sets for alkali metal (K–Fr) and alkaline earth (Ca–Ra) elements. J Chem Phys 2017;147:244106. https://doi.org/10.1063/1.5010587
[75] Yurchenko SN, Thiel W, Jensen P. Theoretical ROVibrational Energies (TROVE): A robust numerical approach to the calculation of rovibrational energies for polyatomic molecules. J Mol Spectrosc 2007;245:126–40. https://doi.org/10.1016/j.jms.2007.07.009
[76] Yurchenko SN, Mellor TM. Treating linear molecules in calculations of rotation-vibration spectra. J Chem Phys 2020;153:154106. https://doi.org/10.1063/5.0019546

[77] Visser O, Visscher L, Aerts PJC, Nieuwpoort WC. Molecular open shell configuration interaction calculations using the Dirac–Coulomb Hamiltonian: The f^6-manifold of an embedded EuO^{9-}_6 cluster. J Chem Phys 1992;96:2910–9. https://doi.org/10.1063/1.461987
[78] Udrescu SM, Brinson AJ, Garcia Ruiz RF, Gaul K, Berger R, Billowes J, Binnersley CL, Bissell ML, Breier AA, Chrysalidis K, Cocolios TE, Cooper BS, Flanagan KT, Giesen TF, de Groote RP, Franchoo S, Gustafsson FP, Isaev TA, Koszorús Á, Neyens G, Perrett HA, Ricketts CM, Rothe S, Vernon AR, Wendt KDA, Wienholtz F, Wilkins SG, Yang XF. Isotope shifts of radium monofluoride molecules. Phys Rev Lett 2021;127:033001. https://doi.org/10.1103/PhysRevLett.127.033001
[79] NIST Atomic Spectra Database, http://www.nist.gov/pml/data/asd.cfm (accessed 15.6.23).
[80] Hanwell MD, Curtis DE, Lonie DC, Vandermeersch T, Zurek E, Hutchison GR. Avogadro: an advanced semantic chemical editor, visualization, and analysis platform. J Cheminformatics 2012;4:17. https://doi.org/10.1186/1758-2946-4-17
[81] Koput J, Carter S, Peterson KA, Theodorakopoulos G. The *ab initio* potential energy surface and vibrational-rotational energy levels of $X^2\Sigma^+$ MgOH. J Chem Phys 2002;117:1539–35. https://doi.org/10.1063/1.1485721
[82] Koput J. *Ab initio* potential energy surface and vibration-rotation energy levels of beryllium monohydroxide. J Comp Chem 2017;38:37–43. https://doi.org/10.1002/jcc.24515
[83] Koechner W. Solid-State Laser Engineering, 6th Revised and Updated Edition, Springer 2006.

CRediT authorship contribution statement

Yuliya Osika: Investigation, Formal analysis, Visualization, Writing – original draft, Writing – review & editing. **Sergey Sharashkin:** Investigation, Formal analysis. **George Pitsevich:** Formal analysis, Project administration. **Maksim Shundalau:** Conceptualization, Formal analysis, Investigation, Writing – original draft, Writing – review & editing, Supervision, Project administration.

Declaration of interests

☒ The authors declare that they have no known competing financial interests or personal relationships that could have appeared to influence the work reported in this paper.

☐The authors declare the following financial interests/personal relationships which may be considered as potential competing interests: